https://doi.org/10.5194/egusphere-2026-1168
Preprint. Discussion started: 18 March 2026


# Dependence of Hadley circulation on the representation of tropical deep convection

Jin-Song von Storch[1], Dian Putrasahan[1], and Cathy Hohenegger[1]
[1]Max Planck Institute for Meteorology, Hamburg, Germany, Bundesstrasse 53, 20146 Hamburg, Germany
**Correspondence:** Jin-Song von Storch (jin-song.von.storch@mpimet.mpg.de)

**Abstract.** Parameterizations of subgrid-scale processes are an important source of bias in climate simulations and uncertainty in climate projections. Both the bias and the uncertainty can be reduced by resolving the most energetic small-scale processes based on the first principles via increasing model resolution, as oppose to relying on empirical or ad hoc (though physically motivated) parametrizations. We made a first step in this direction using a suite of time-slice and fixed-season experiments, specifically designed to deal with the heavy computational costs encountered when using a global 5km model for climate and climate change simulations. We concentrate on the effect of the representation of deep convection for the Hadley Circulation (HC) and its response to warming.

We find that the time-mean state of HC is sensitive to the representation of deep convection: The HC is significantly weaker and the deep convection is significantly reduced in the case when deep convection is resolved instead of parametrized. Resolving convection leads to less heavy rain and less rain in the ascending branch of the HC—consistent with a weaker HC—but more total precipitation when taking also light rain into account. As a response to a 4K global warming, the HC becomes broader, deeper, and weaker, no matter whether convection is resolved or parameterized. There is an indication that the weakening of HC is further intensified when deep convection is resolved. As a response to the warming, heavy rain and the rain associated with the HC ascending branch become stronger regardless of convection representation, while the total precipitation is more strongly enhanced when convection is resolved.

## 1 Introduction

Modelling atmospheric circulation has experienced two regime shifts. The first one happened in the 1960s, when atmospheric models started to be run at a resolution of a few 100 of kms (Smagorinsky et al., 1965). With this shift, mid-latitude synoptic-scale cyclones resulting from baroclinic instability could be explicitly resolved by solving the underlying primitive equations. The second regime shift happened around the 2005's with the first atmospheric simulation conducted with a grid spacing of the order of 10 km, globally (Satoh et al., 2005; Miura et al., 2007). With this second shift, tropical deep convection could be explicitly resolved instead of being parameterized, and interactions between the small and synoptic scales of motion explicitly

https://doi.org/10.5194/egusphere-2026-1168
Preprint. Discussion started: 18 March 2026


represented. As tropical deep convection together with other diabatic processes constitute the engine of the Hadley circulation (HC), explicitly resolving deep convection can impact the representation of the time-mean HC and the response of HC to global warming. This paper quantifies these impacts by comparing HC and its response to a global warming found in simulations with resolved versus parameterized deep convection.

The response of the HC to a global warming has been extensively studied using both reanalyses and climate model simulations. Regarding the width of HC, the IPCC Sixth Assessment Report (AR6) concludes that "It is likely that human influence has contributed to the poleward expansion of the zonal mean Hadley Cell in the Southern Hemisphere since the 1980s". However, it is less clear regarding the strength of HC. While reanalyses tend to exhibit a HC strengthening (Nguyen et al., 2013; Stachnik and Schumacher, 2011; Žiga Zaplotnik et al., 2022), climate models exhibit a weakening (Simpson et al., 2025; Chemke and Polvani, 2019; Chemke and Yuval, 2023). While there are indications that the reanalyses may actually be in error (Chemke and Polvani, 2019; Chemke and Yuval, 2023), radiosonde observations show a neutral trend in northern HC strength over the 1980-2022 period (Pikovnik and Zaplotnik, 2025). The picture becomes even more complex when taking the seasonality of the HC into account (Lionello et al., 2024). Different mechanisms have been examined with respect to their roles in affecting the HC response. In a recent paper, Chemke and Polvani (2021) showed that the HC weakening results from a combination of an increase in tropical static stability, partially offset by an increase in the latitudinal gradient of latent heating. Frierson (2007) showed that tropical circulation is sensitive to idealized convection schemes. To date, the impact of the representation of deep convection—whether treated explicitly or parameterized—on the Hadley circulation (HC) has not, to our knowledge, been systematically examined. Moreover, its role in shaping the HC response to global warming has not been addressed. This study provides a first assessment of whether, and to what extent, both the climatological mean HC and its response to global warming depend on the representation of tropical deep convection.

When quantifying differences in HC and HC response to global warming due to different representations of deep convection, one needs to deal with internal variability that masks the differences caused by different representations. To limit the internal variability, the HC is often estimated from velocities averaged over a long time period, usually over 20 or 30 years. As it is still challenging to run a km-scale model over decades, we consider in this paper perpetual January simulations. A simulation of one year length contains then 12 Januaries. The drawback of our approach is that we can only study the January HC, which has its ascending branch in the Southern Hemisphere. Section 2 describes the model and experiments used, as well as the metrics used to characterize HC and tropical deep convection. The results regarding the differences in both the time-mean HC and the mean HC response to a 4K surface warming due to parametrized versus resolved convection are represented in section 3. Conclusions are given in section 4.

## 2 Experiments and metrics

### 2.1 ICON-Atmosphere and perpetual January experiments

We employ the atmosphere component of the ICOsahedral Non-hydrostatic model (ICON), once integrated in its low-resolution configuration (Giorgetta et al., 2018) and once in its so-called Sapphire configuration (Hohenegger et al., 2023). ICON solves

https://doi.org/10.5194/egusphere-2026-1168
Preprint. Discussion started: 18 March 2026


for an atmosphere with a condensible (water) component the fully compressible Navier-Stokes equations on a triangular grid (Zängl et al., 2015). Land surface processes are modelled by the light version of the JSBACH land surface model version 4, similar to Reick et al. (2021). The low-resolution configuration uses a resolution of R2B6, which corresponds to a resolution of approximately 40 km, and 72 vertical levels. It uses parameterizations for radiation, shallow and deep convection, cloud cover, microphysics, with the prognostic hydrometeors water vapor, cloud water and cloud ice, turbulence, orographic and non-orographic gravity waves. Convection is parameterized by the Tiedtke (1989) mass flux scheme with updates by Nordeng (1994). For more detail on the parameterizations used, see Giorgetta et al. (2018). The time step is 120 s, except for radiation which is called every hour. The Sapphire configuration uses a resolution of R2B9, approximately 5 km, and 90 vertical levels. Only three parameterizations are retained: radiation, microphysics, with the prognostic hydrometeors water vapor, cloud water, cloud ice, rain, snow and graupel, as well as turbulence. More details on the employed parameterizations are in Hohenegger et al. (2023). The time step is 60 s, except for radiation which uses a time step of 20 minutes. Note that only the radiation parameterization is identical in the two configurations.

Two pairs of perpetual January experiments, referred to as CTL (control) and 4K, are performed with each of the two ICON configurations. The experiments use the same January solar insolation, but different lower boundary conditions derived from MPI-ESM simulations (Mauritsen et al., 2019; Putrasahan et al., 2021). The CTL experiments use as the lower boundary conditions the fields of sea surface temperature (SST) and sea ice cover (SIC) obtained by averaging over 40 Januaries taken from the piControl simulation conducted with the MPI-ESM forced by 1850 $CO_2$ concentration. The 4K-experiments use the SST- and SIC-fields obtained by averaging over 40 Januaries taken from the last 20 Januaries (2080-2099) of two climate change simulations with the same MPI-ESM under the SSP585 scenario. During this 20-year period, the global mean surface temperature is about 4°K warmer than that in the control run. $CO_2$ and aerosols are not changed between the experiments. $CO_2$ is set to a constant and aerosols to their January climatology (Kinne et al., 2013). The land surface characteristics, such as soil properties, albedo, leaf area index, represent mean January conditions and are kept the same for all simulations. These land conditions are derived from the same datasets as used in the past in the MPI-ESM (Mauritsen et al., 2019). These datasets have an original resolution of 0.5°. In contrast, orography is derived from the Global Land One-km Base Elevation Project (GLOBE), with a nominal resolution of about 1km. In all experiments, soil moisture and soil temperature as well as the atmospheric fields are initialized from ECMWF IFS analysis taken on 1st January 1979.

The experiments performed with the 40km-ICON cover 120 Januaries, and those with 5km-ICON cover 12 Januaries. Most of the results are based on averages over 12 Januaries, which are considered to be representative for describing the 10-year mean January conditions. The 120 Januaries simulated by 40km-ICON are used to build statistics, which can describe how likely a quantity simulated by the 5km-ICON can be observed under the hypothesis that there is no difference between 40km- and 5km ICON. A summary of the experiments is given in Tab. 1.

Experiments CTL-40 and CTL-5 are forced with the same boundary conditions and the same radiative forcing. The difference between the two will be used to quantify the impact of resolved versus parameterized deep convection on the *time-mean HC*. Although the two model configurations differ more than just by the treatment of convection, we assume that the treatment of convection plays a key role. The responses of HC to global warming will be described by the difference between 4K-40

https://doi.org/10.5194/egusphere-2026-1168
Preprint. Discussion started: 18 March 2026


| experiment names | horiz. resolution | forcing | length of simulation |
|---|---|---|---|
| CTL-40 | 40km | SST/SIC under 1950 condition | 120 months |
| 4K-40 | 40km | SST/SIC under +4°K condition | 120 months |
| CTL-5 | 5km | SST/SIC under 1950 condition | 12 months |
| 4K-5 | 5km | SST/SIC under +4°K condition | 12 months |

**Table 1.** Names and some basic features of the experiments performed.

and CTL-40, and that between 4K-5 and CTL-5. These two responses will be used to quantify the impact of resolved versus parametrized deep convection on the *HC's response* to global warming.

### 2.2 Metrics

As in most previous studies (see e.g. Pikovnik et al. (2022); Baldassare et al. (2023); Lionello et al. (2024)), the HC is described by the time-mean mass-weighted zonal-mean stream function $\Psi$ in the latitude-pressure ($\varphi$, $p$) plane

$$\Psi(\varphi,p) = \left\langle 2\pi R\cos(\varphi)/g \int_0^p [v](\varphi,p')\, dp' \right\rangle, \tag{1}$$

where $\langle \cdot \rangle$ indicates an average over 12 Januaries, $[\cdot]$ zonal mean, $R$ is Earth's radius, and $g$ gravity. $\Psi$ simulated by both the 40km-ICON and the 5km-ICON reveals the same basic features of HC in boreal winter (Fig.1), with the ascending branch located near 15°S and the descending branch near 30°N.

https://doi.org/10.5194/egusphere-2026-1168
Preprint. Discussion started: 18 March 2026


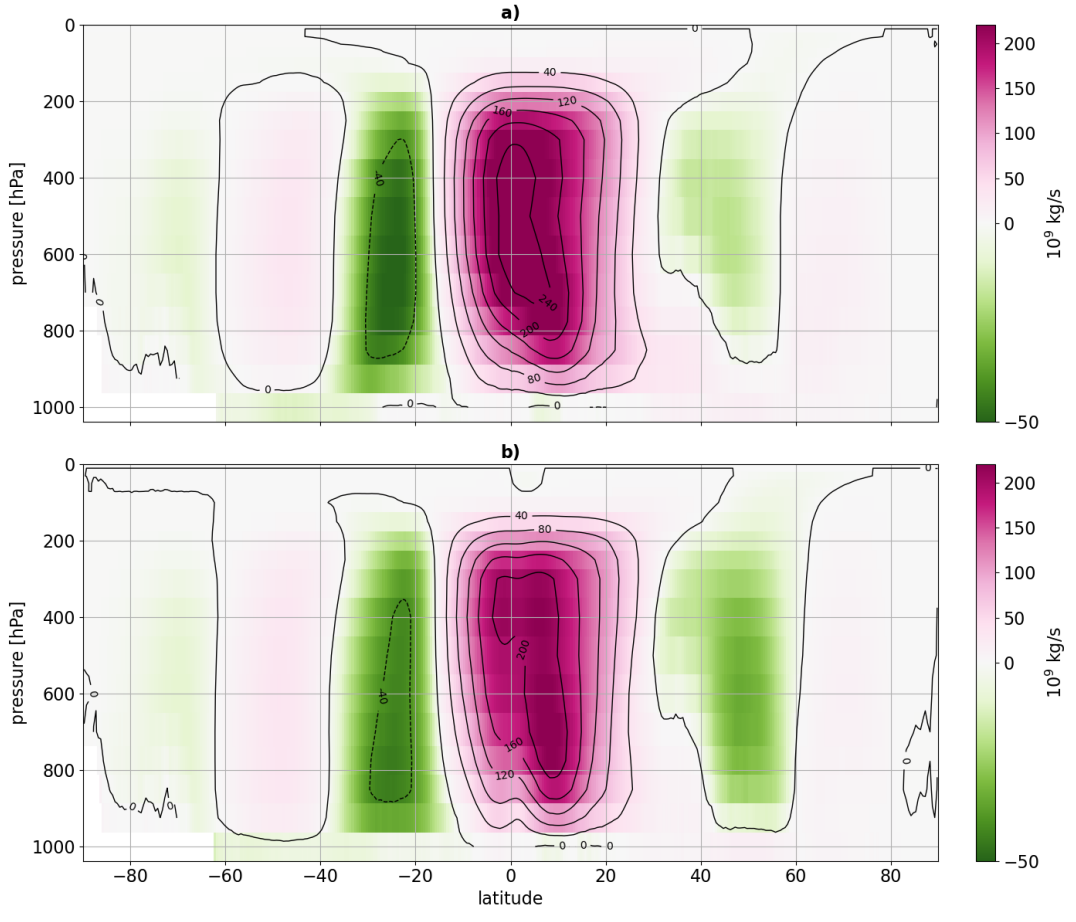


**Figure 1.** Mass stream function Ψ as defined in Eq.(1) obtained from experiments a) CTL-40 and b) CTL-5.

https://doi.org/10.5194/egusphere-2026-1168
Preprint. Discussion started: 18 March 2026


Metrics are used to quantify three properties of a simulated HC, the width, the strength and the height, mostly based on $\Psi$. For each of the three properties, several metrics are considered, since metrics that rely on single-point values in the $\varphi - p$ plane can produce unreliable trends (Pikovnik et al., 2022). The width of a HC is described by $\Delta\varphi_p = \varphi_{n,p} - \varphi_{s,p}$, where $\varphi_{n,p}$ and $\varphi_{s,p}$ are the northern and southern edge of the HC, defined using $\Psi$ at pressure level $p$. North of 50°S, the latitude of the first zero-crossing of this $\Psi$ marks the southern edge $\varphi_{s,p}$, the latitude of the second zero-crossing the dividing line of the southern and northern cells $\varphi_{0,p}$, and that of the third zero-crossing the norther edge $\varphi_{n,p}$. Two values of $p$, 400 and 500 hPa, are considered.

The strength of HC is described using both $\Psi$ and area-weighted mean of vertical velocity $w$. The one using $\Psi$ is defined as the maxima of $\Psi$ at a selected pressure level $p$, $\Psi_{max,p}$. Again, two values of $p$, 400 and 500 hPa, are considered. The strength of a HC is also influenced by $w_{asc}$, defined as the vertical velocity at $p$=500 hPa averaged over the area of the ascending branch of the Hadley cell. The ascending area is defined as the latitudinal band extending from $\varphi_{min,p}$ to $\varphi_{max,p}$, where $\varphi_{min,p}$ and $\varphi_{max,p}$ are, respectively, the latitudes of $\Psi_{min,p}$ and $\Psi_{max,p}$ (i.e. the latitudes of the darkest green and the darkest magenta at $p$ =500 hPa in Fig.1).

The height of a HC is described by the pressure level at which the mass-weighted stream function with a given value of $\Psi$ is located, $h_\Psi$. Four values of $\Psi$, $\Psi$=20, 10, 5 and 3 in the unit of $\times 10^{10}$ kg/s, are considered.

Since this paper focuses on the effects of parameterized and resolved convection on HC, three additional metrics based on mean precipitation are considered. $P_{all}$ is the global area-weighted mean precipitation. It quantifies the total precipitation, regardless of its intensity. $P_{hvy}$ is the area-weighted mean precipitation that excesses 10 mm/day (red lines in Fig.6 and Fig.7). It quantifies the heavy precipitation, which tends to be located in the tropics. Finally, $P_{asc}$ is the area-weighted mean precipitation over the ascending latitudinal band of the Hadley cell, which extends from $\varphi_{min,p}$ to $\varphi_{max,p}$ with $p = 500$ hPa and is the same band used to define $w_{asc}$. $P_{asc}$ is expected to be directly associated with the strength of the Hadley cell. Being resulting from the rain in the ascending band, $P_{asc}$ indicates the strength of latent heating due to convection in that latitudinal band.

## 3 Results

### 3.1 Time-mean January HC

The metrics defined in section 2 are calculated using mass stream function or vertical velocity and precipitation averaged over 12 Januaries. Such a metrics can vary strongly due to internal variability. To quantify the variations associated with a metrics, 200 values of the metrics are generated, each based on the mean of 12 Januaries randomly selected from the pool of total 120 Januaries produced by experiment CTL-40 / 4K-40. The probability of observing certain value of a metrics is then depicted by a box plot (see e.g. Fig.2), where the whiskers extend from the 5th to the 95th percentile assuming that the considered metrics is normally distributed. From experiment CTL-5 / 4K-5, we have only one value of each metrics. This value will be considered as significantly different from that in CTL-40 / 4K-40, if it lies outside the whiskers, which corresponds to a probability of less than 10% of being also found in CTL-40 / 4K-40 (see also the caption of Fig.2).

https://doi.org/10.5194/egusphere-2026-1168
Preprint. Discussion started: 18 March 2026


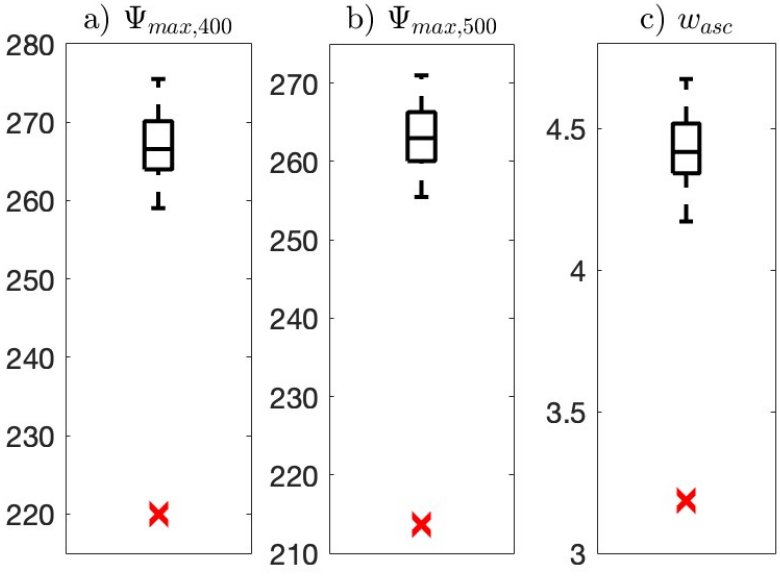


**Figure 2.** Strength of time-mean HC described by the maximum of mass weighted stream function $\Psi_{max,p}$ at $p$ =400 and 500 hPa in a) and b), and by the vertical velocity $w_{asc}$ averaged over the ascent branch of the HC at 500 hPa in c), simulated by CTL-40 (box plots) and CTL-5. $\Psi_{max,400}$ and $\Psi_{max,500}$ are in $\times 10^9$ kg/s. Vertical velocity are in mm/s. For each metrics, 200 values are obtained from experiment CTL-40 and their statistics are described by a box with whiskers. A single value is obtained from experiment CTL-5. The 200 values are derived from 200 $\Psi$, each obtained by averaging 12 randomly selecting Januaries from a pool of total 120 Januaries. The edges of a box indicates the 25th to the 75th percentile. The horizontal line inside the box indicates the median. The length of a whisker corresponds to 5% and 95% percentiles, assuming that the metrics is normally distributed.

The mean HC simulated by 40km-ICON differs significantly from that simulated by the 5km-ICON. The difference pertains mainly to the strength. The maxima of $\Psi$ at 400 and 500 hPa are about $50\times10^9$kg/s weaker in CTL-5 than in CTL-40 (Fig.2a-b). The vertical velocity in the ascending branch of HC, $w_{asc}$, is around 4.4 mm/s in CTL-40, but reaches only about 3.2 mm/s in CTL-5 (Fig.2c). The smaller value of $w_{asc}$ in CTL-5 than in CTL-40 results both from smaller ascent-area-integrated $w$, which is about $4.2\times10^{11}$ m$^3$/s in CTL-5 and $4.6\times10^{11}$ m$^3$/s in CTL-40, and from the wider ascent area, which is about $1.3\times10^{14}$ m$^2$ in CTL-5 and $1.0\times10^{14}$ m$^2$ in CTL-40. Thus, both the maxima of $\Psi$ and $w_{asc}$ indicate a significantly weaker HC in CTL-5 than in CTL-40.

This weakening is further confirmed by the metrics describing the HC height (Fig.3). The isoline of $\Psi = 20 \times 10^{10}$ kg/s and that of $\Psi = 10 \times 10^{10}$ kg/s are located at a lower altitude (i.e. higher pressure level) in CTL-5 than in CTL-40 (Fig.3a-b), whereas the isoline of $\Psi = 5 \times 10^{10}$ kg/s and that of $\Psi = 3 \times 10^{10}$ kg/s reach a higher altitude (lower pressure level) in CTL-5 than in CTL-40. Thus, the distance between two isolines, one close to and the other further above the stream function maximum, is larger in CTL-5 than in CTL-40. The velocity of the northward flow, which is proportional to the reciprocal of

https://doi.org/10.5194/egusphere-2026-1168
Preprint. Discussion started: 18 March 2026


this distance and hence proportional to the vertical gradient of $\Psi$, is then smaller in CTL-5 than in CTL-40. As all CTL-5 metrics lie outside the range covered by the whiskers of the CTL-40 metrics, it is unlikely to obtain them would the resolved deep convection have the same effect as the parametrized deep convection.

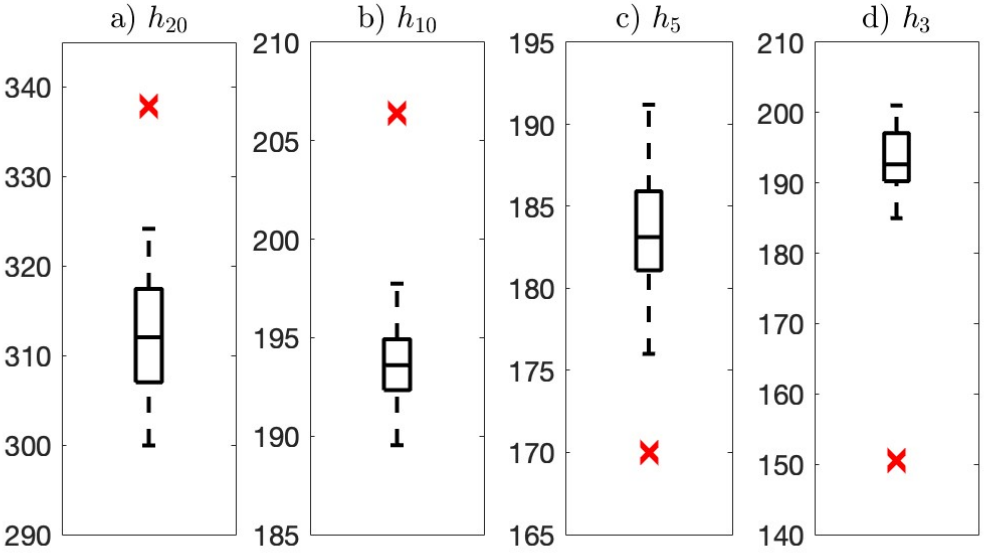


**Figure 3.** Same as Fig.2, but for the height of time-mean HC described by metrics $h_{20}$, $h_{10}$, $h_5$, and $h_3$, which are defined as the altitudes of the isoline of $\Psi$ with $\Psi = 20 \times 10^{10}$, $10 \times 10^{10}$, $5 \times 10^{10}$, and $3 \times 10^{10}$ kg/s. The unit of $h_{20}$, $h_{10}$, $h_5$, and $h_3$ is hPa.

The difference in width (Fig.4) is much less significant than the difference in strength. Both $\Delta\varphi_{400}$ and $\Delta\varphi_{500}$ in CTL-5, which are about 67.2 and 67.7 degrees latitude, are narrower than at least the 25% percentiles found in CTL-40. The probability of obtaining these CTL-5 value in CTL-40 is hence small. Together, Fig.2-Fig.4 show that the weaker HC simulated by CTL-5 is associated with a higher reaching HC and a tendency to be narrower.

The weaker HC in CTL-5 than in CTL-40 is accompanied by weaker area-weighted mean precipitation as measured by significantly smaller values of $P_{hvy}$ and $P_{asc}$ in CTL-5 than in CTL-40 (Fig.5a and b). The mean heavy rainfall $P_{hvy}$ decreases from about 17 mm/day in CTL-40 to about 14 mm/day in CTL-5. The mean precipitation within the ascending branch of the Hadley cell $P_{asc}$ decreases from about 6.5 mm/day in CTL-40 to about 5.7 mm/day in CTL-5. The decrease results from a somewhat stronger precipitation intensity but a much larger ascent area in CTL-5 than in CTL-40: The ascent-area-integrated precipitation rate is $7.6\times10^{11}$ m$^3$/day in CTL-5 and $6.7\times10^{11}$ m$^3$/day in CTL-40, whereas the ascent area is $1.3\times10^{14}$ m$^2$ in CTL-5 and $1.0\times10^{14}$ m$^2$ in CTL-40. This intuitively makes sense. Precipitation is a measure of how much latent heat is released. Less mean precipitation in the ascending branch of the HC means that less heat is released within the latitudinal band of ascending motion, which results in a reduction of the latitudinal difference in latent heating and a weaker HC (Chemke and Polvani, 2021). Likewise, if there is less precipitation in the ascending branch of the HC, this means that less mass was

https://doi.org/10.5194/egusphere-2026-1168
Preprint. Discussion started: 18 March 2026


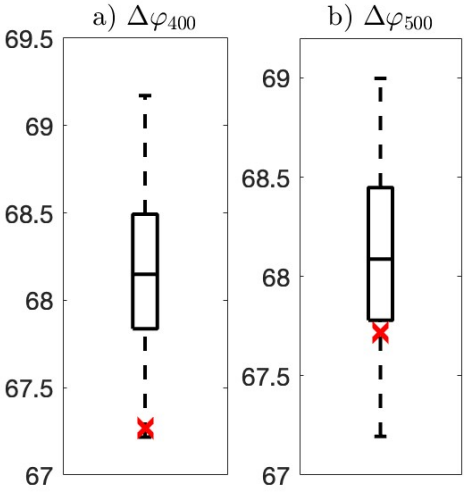


**Figure 4.** Same as Fig.2, but for the width of time-mean HC described by $\Delta\varphi_{400}$ and $\Delta\varphi_{500}$ based on mass weighted stream function $\Psi(\varphi, p)$ for $p$ at 400 and 500 hPa. Unit is in degree latitude.

transported upward and that the convective mass flux is smaller. A smaller convective mass flux is often associated with a weaker HC (Held and Soden, 2006). We conclude that when convection is explicitly resolved, there is less mean precipitation within the ascending branch of the HC, the vertical velocity is correspondingly slower and the HC less intense.

In contrast, if we just look at total mean precipitation $P_{all}$ (Fig. 5c ), we see a different picture. $P_{all}$ is actually significantly larger in CTL-5 than in CTL-40. Given that heavy rains are weaker in CTL-5 than in CTL-40 (Fig. 5a), Fig. 5c suggests there are a lot more light rains in CTL-5 than in CTL-40. That the ascent-area-integrated precipitation $P_{asc}$ (numbers given above) is stronger in CTL-5 than in CTL-40 can be a direct consequence of more light rains in CTL-5 than in CTL-40. It appears that the increase in light rains is not relevant for HC strengthening.

Finally, looking at the spatial pattern of precipitation (Fig.6a and Fig.7a), in CTL-40, the major tropical rainfall is located south of the equator, especially over the western Pacific. In contrast, in CTL-5, the major tropical rainfall is located on both sides of the equator. This is consistent with the wider ascending branch of the HC in CTL-5. Other differences concern the stronger rainfall over Kuroshio and Gulf Stream but weaker rainfall over tropical Africa and South America in CTL-5 than in CTL-40.

### 3.2 Response of January HC to 4k-warming

The response to the 4K warming is described by the difference in a metric or a variable simulated by ICON under the +4K condition and that under the 1950 condition (4K minus CTL). A positive difference indicates an increase, and a negative one indicates a decrease of the considered metric / variable. Our results may be compared with CMIP6 projections (which

https://doi.org/10.5194/egusphere-2026-1168
Preprint. Discussion started: 18 March 2026


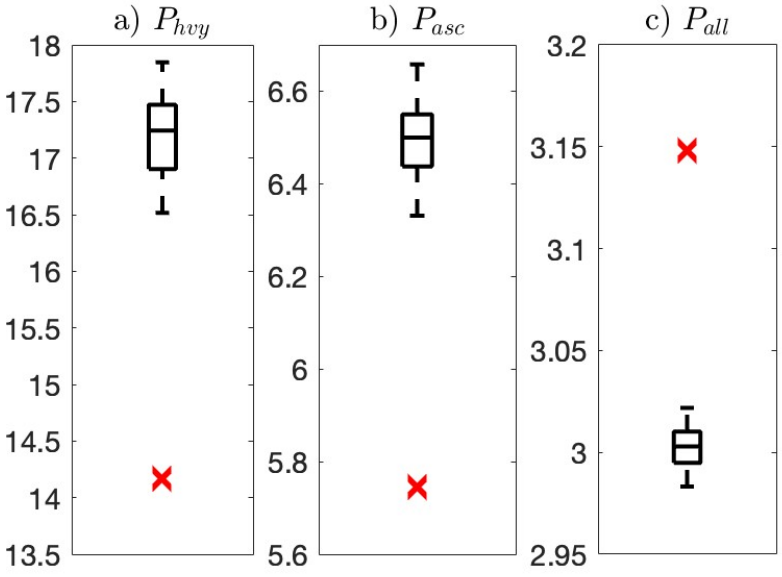


**Figure 5.** Same as Fig.2, but for the precipitation metrics $P_{hvy}$ defined as the mean precipitation over the area with precipitation stronger than 10 mm/day (indicated by the red contours in Fig.6 and Fig.7), $P_{asc}$ defined as the mean precipitation over the ascending branch of the HC, and $P_{all}$ defined as the global mean precipitation. Unit is mm/day.

180 themselves carry substantial uncertainty) in a qualitative but not in a quantitative manner, owing to differences in model configuration—AMIP-style perpetual January rather than a fully coupled model with an annual cycle—and in forcing, namely prescribed SST and SIC under a 4 K warming instead of a specific greenhouse-gas concentration scenario.

Consistent with most CMIP6 models, both the 5km and the 40km ICON simulate a widening of HC under the 4K warming (Fig.8). The median of the increase in the width is about 2 degrees in the 40km simulations. A similar increase is also found in 185 the 5km simulation. The response in HC width does not significantly depend on the representation of deep convection.

The response of HC strength simulated by the 40km ICON is a weakening with a median of about -10 $\times 10^9$ kg/s when judged by $\Psi_{max,400}$ (Fig.9a), but essentially neutral with the median close to zero when judged by $\Psi_{max,500}$ (Fig.9b). The response of HC strength simulated by the 5km ICON is not significantly different from that simulated by the 40km ICON, although the weakening simulated by the 5km ICON is stronger than the medians of both $\Psi_{max,400}$ and $\Psi_{max,500}$ found in 190 the 40km ICON. The response of $w_{asc}$ in the 5km runs is an increase of about +0.2 mm/s. Given the strong variability in vertical velocity, a consideration of the meridional profile of zonal-mean vertical velocity reveals that the positive response of $w_{asc}$ is associated with a larger meridional extent of the major ascending velocity in 4K-5 than in CTL-5. We conclude that the response of HC strength exhibits a slight weakening, with a weak indication that the weakening is enhanced when deep convection is resolved rather than parameterized.

https://doi.org/10.5194/egusphere-2026-1168
Preprint. Discussion started: 18 March 2026


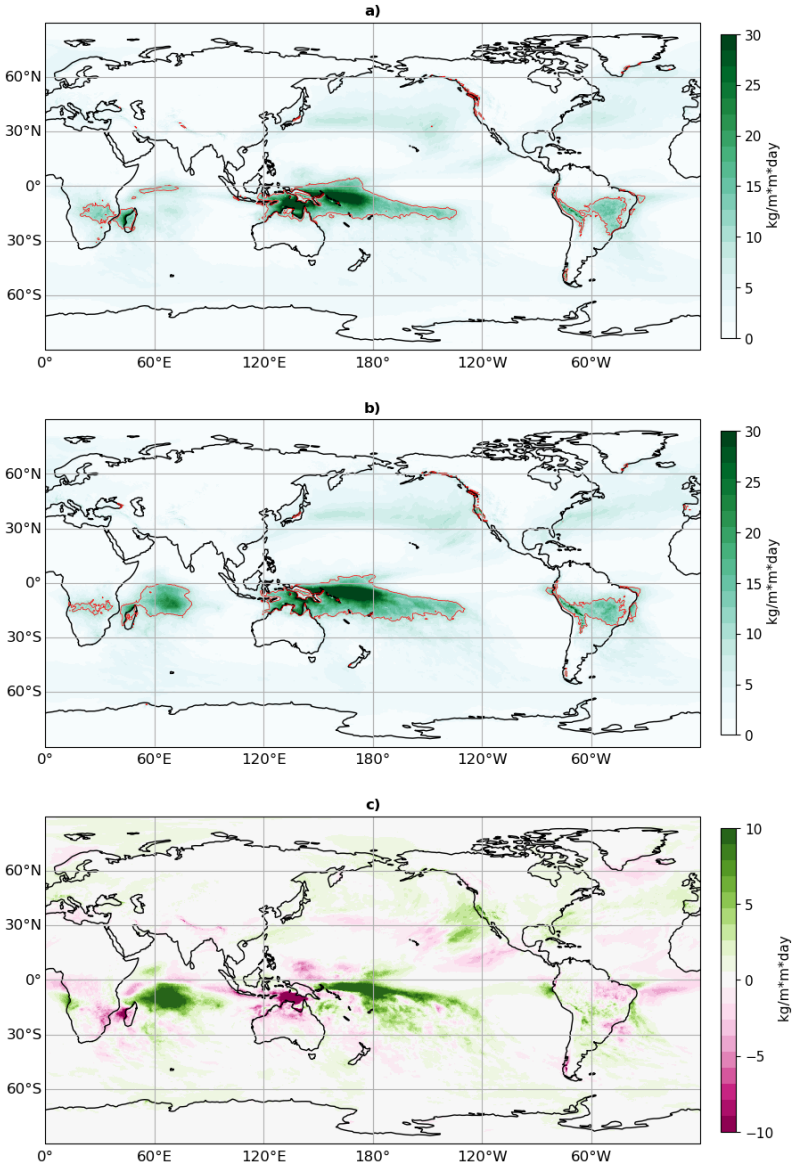


**Figure 6.** Daily precipitation average over 12 Januaries in experiment CTL-40 in a), in 4K-40 in b), and their difference (4K-40 minus CTL-40) in c). Unit: mm/day.

195 The above conclusion is supported by the responses in HC height (Fig.10). The 40km ICON simulates an increase in the heights (decrease in pressure) of the four considered stream function isolines, with all of them having negative medians. Three of the four, namely those having the values of $10 \times 10^9$ kg/s, $5 \times 10^9$ kg/s, and $3 \times 10^9$ kg/s (Fig.10b-c), show significantly

https://doi.org/10.5194/egusphere-2026-1168
Preprint. Discussion started: 18 March 2026


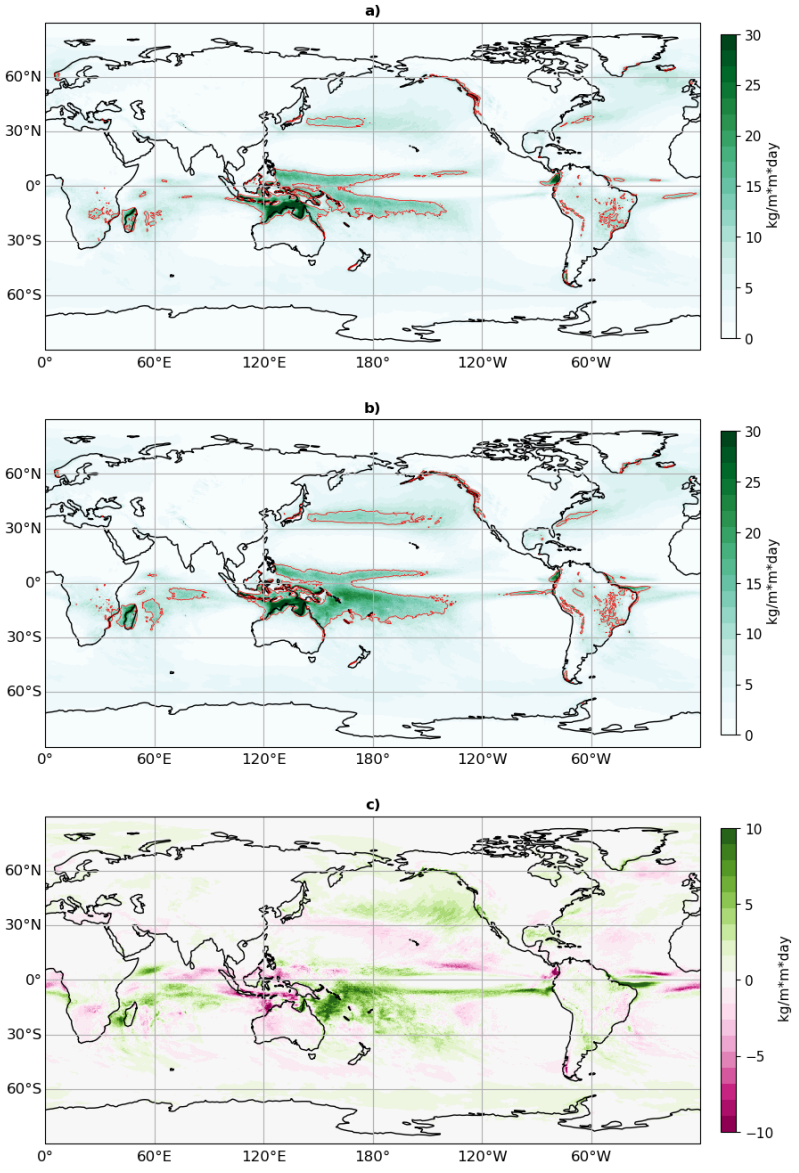


**Figure 7.** Same as Fig.6, but derived from precipitation in CTL-5 and 4K-5.

stronger increase in the heights in 5km than in 40km run, while the height of the isoline having the value of $20 \times 10^9$ kg/s ($h_{20}$) reveals comparable response in 40km and 5km runs. This suggests that the distance from $h_{10}$, $h_5$ and $h_3$ to $h_{20}$ is significantly increased, indicating a decrease in vertical gradient of stream function, and with that a reduction in the velocity of the northward flow of the HC.

https://doi.org/10.5194/egusphere-2026-1168
Preprint. Discussion started: 18 March 2026


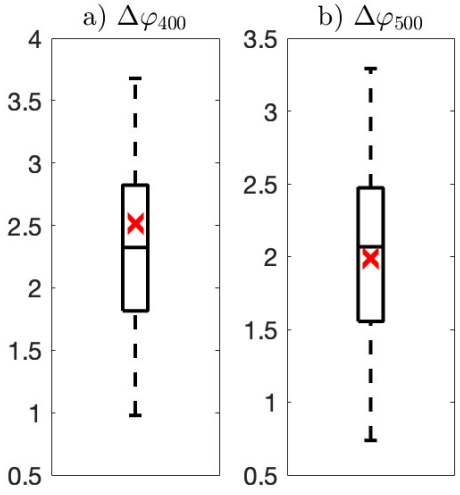


**Figure 8.** Same as Fig.4, but for the response (4K minus CTL) of HC width to the 4K warming, as described by the metrics $\Delta\varphi_{400}$ and $\Delta\varphi_{500}$.

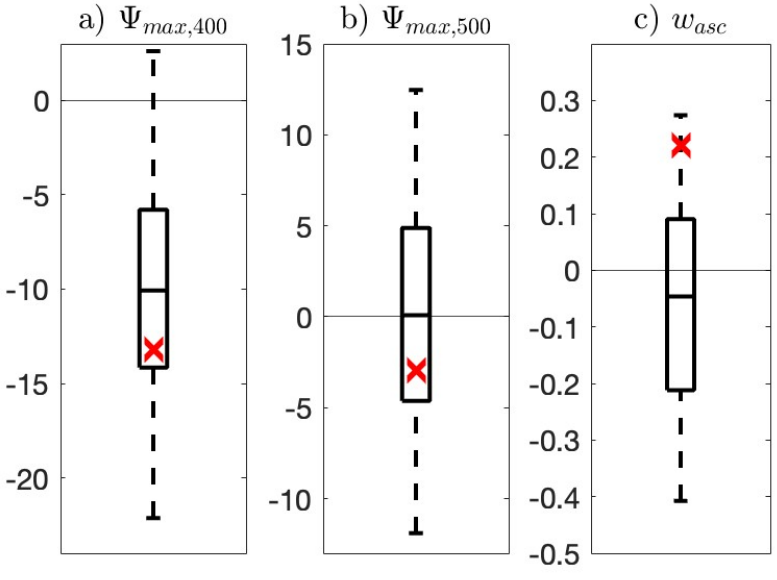


**Figure 9.** Same as Fig.2, but for the response (4K minus CTL) of HC strength to the 4K warming, as described by the metrics $\Psi_{max,400}$, $\Psi_{max,500}$, and $w_{asc}$.

https://doi.org/10.5194/egusphere-2026-1168
Preprint. Discussion started: 18 March 2026


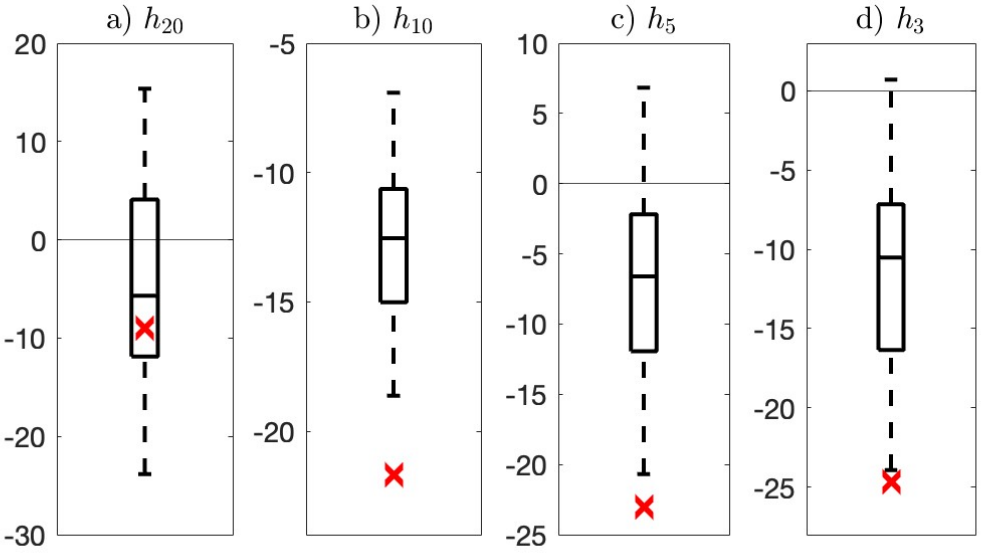


**Figure 10.** Same as Fig.3, but for the response (4K minus CTL) of HC height to the 4K warming, as described by the metrics $h_{20}$, $h_{10}$, $h_5$, $h_3$.

The extent to which the HC response relates to that of precipitation is investigated with Fig.11a and b. When convection is parameterized (40km simulation), the response of $P_{hvy}$ and $P_{asc}$ is an increase, described by a median of about 0.4 mm/day and 0.8 mm/day, respectively. Both indicate an intensification of precipitation. When convection is resolved (5km simulation), the response of $P_{hvy}$ is about 0.2 mm/day, and that of $P_{asc}$ is about 0.6 mm/day. An increase in precipitation is expected from energetics and thermodynamic constraints (Allen and Ingram, 2002; Held and Soden, 2006). For a 4-K SST increase, $P_{asc}$ increases around 3% per Kelvin in ICON. As explained in Held and Soden (2006), the slower increase of precipitation with warming compared to boundary layer humidity, which increases following Clausius-Clapeyron, implies a weakening of the HC. This is consistent with the ICON response, both at 40 and 5 km. Held and Soden (2006) conclusion assumes that the convective mass flux only depends upon precipitation and boundary layer humidity. As recently shown by Williams and Jeevanjee (2025), the relative humidity at cloud base also has to be taken into account. In the ICON simulations, the relative humidity at cloud base does not change much. Hence, the increase in precipitation associated with the HC and the weakening of the Hadley cell can be explained by simple thermodynamic arguments and, as the changes in the controlling parameters are not significantly different between 40km and 5km, the changes in HC intensity remain comparable.

The effect of the convection representation becomes more detectable when considering the response of total precipitation $P_{all}$. Fig.11c shows that this is noticeably stronger in 5km than in 40km runs. In relative terms, the increases are 3.2% per Kelvin and 2.5% per Kelvin for the 5km and the median of the 40km simulation. Given that the response of the heavy rain

https://doi.org/10.5194/egusphere-2026-1168
Preprint. Discussion started: 18 March 2026


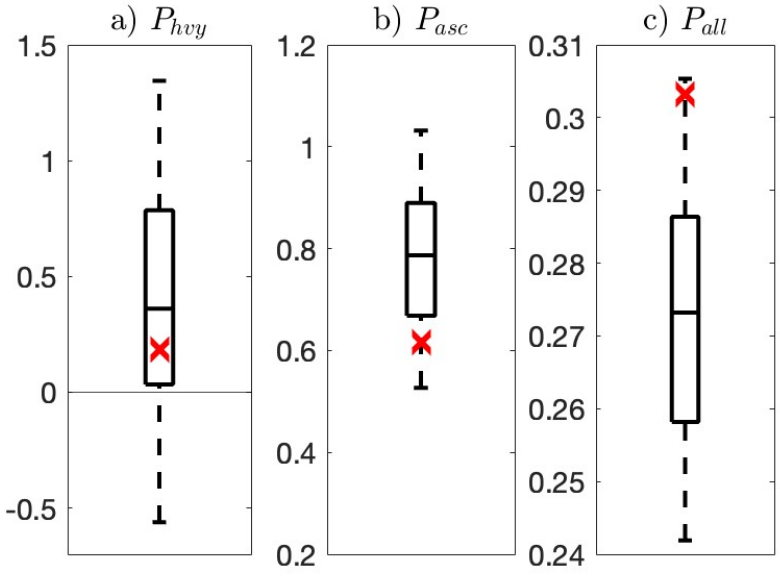


**Figure 11.** Same as Fig.5, but for the response (4K minus CTL) of precipitation to the 4K warming, as described by the metrics $P_{hvy}$, $P_{asc}$ and $P_{all}$.

$P_{hvy}$ is not significantly different between 5km and 40km, the response of the total precipitation shown in Fig.11c suggests that it is especially the light precipitation that increases more under global warming when convection is resolved.

The geographical distribution of precipitation response simulated by the 40km ICON (Fig.6c) does differ noticeably from the 5km one (Fig.7c). While the response in the 40km run reveals a strong increase in precipitation in both the tropical southern Indian Ocean and the tropical South Pacific, the response in the 5km run shows a strong increase only in the tropical South Pacific. Note that in CTL (Fig.6a and Fig.7a), both the 40km and the 5km ICON simulate only strong precipitation in the Pacific. It is only under the 4K warming that the 40 km ICON simulates strong precipitation also in the Indian Ocean (Fig.6b). There are also more specific differences regarding the responses in the Pacific. While the maximum response simulated by the 40km ICON is concentrated in a narrow rain belt running essentially zonally west of the dateline but southeastward east of the dateline, the maximum response simulated by the 5km ICON is concentrated around the Coral Sea northeast of Australia. The 5km ICON generates also a distinct zonal band of response near 7°S, stretching from Solomon Islands to the coast of South America. It is unclear whether and to what extent the different geographical distributions of deep convection affect or are related to the HC response.

All together, both the 40km and the 5km ICON simulate a broader, deeper, and weaker HC as response to the 4K global warming. The difference between 40km and 5km runs in terms of their sensitivity to global warming is much smaller than the difference in their basic state. Only the difference in the HC height is statistically significant, pointing to a stronger weakening

https://doi.org/10.5194/egusphere-2026-1168
Preprint. Discussion started: 18 March 2026


in HC strength when deep convection is resolved than when it is paramtrized. A significant stronger weakening cannot be detected using the metrics based on stream function maximum and vertical velocity in HC ascending branch, nor using the metrics that describe the HC width. It can also not be detected using the precipitation metrics $P_{hvy}$ and $P_{asc}$.

## 4 Summary

The dependence of the Hadley Cell (HC) on the representation of tropical deep convection is investigated using two configurations of ICON under perpetual January conditions. One has a resolution of 40km and is equipped with a convection parametrization. The other has a resolution of 5km and can directly resolve the tropical deep convection. The same lower boundary conditions, one corresponding to 1950 conditions and the other to a 4K warming, are applied to simulations with both configurations of ICON.

Regarding the time-mean base state, the HC strength depends strongly on the representation of tropical deep convection. The HC is much weaker when deep convection is resolved than when it is parametrized. The weaker HC is characterized by a smaller value of the stream function maximum, as well as by a weaker poleward velocity in the upper troposphere as indicated by a larger distance between stream function lines close to and further above its maximum, and by a smaller vertical velocity in the region of the ascending branch of the HC. The weaker HC corresponds to weaker deep convection—characterized by less heavy rain and less rain within the ascending branch—obtained when convection is resolved than when convection is parametrized. When taking also light rain into account, a larger amount of total precipitation is generated when convection is resolved than when it is parameterized. There is also a distinct difference between the precipitation pattern: While the precipitation simulated by parametrized deep convection is located mainly south of the Equator, that simulated by resolving deep convection also forms a secondary band in the Northern hemisphere over the western Pacific.

Regarding the response to the 4K warming, the differences between the two configurations of ICON are subtle and much smaller than those found for the time-mean base state. The HC weakens. The weakening of the HC under the 4K warming is most clearly indicated by the metrics describing the height of stream function isolines, not so clear by the stream function maximum, especially that at 500 hPa. With respect to the height metrics, ICON that resolves deep convection simulates a stronger weakening in HC than ICON that employs a convection parametrization. Heavy precipitation and precipitation within the HC ascending branch increase similarly in both configurations. As they increase less than Clausius-Clapeyron, one would expect a weakening of the HC, as obtained. Noticeable dependence on convection representation is found for the total precipitation, when light rain is taking into account. The increase in total precipitation under 4K warming is enhanced when convection is resolved. Noticeable dependence on convection representation is also found regarding the pattern of precipitation response. One major difference is that two centers of precipitation response, one in the Pacific and one in the Indian Ocean, are simulated by ICON with parametrized convection, whereas only one, namely that in the Pacific, is simulated by ICON that resolves convection.

https://doi.org/10.5194/egusphere-2026-1168
Preprint. Discussion started: 18 March 2026


*Code and data availability.* A description of the simulations and the scripts used to produce the main results of this paper will be archived in the publication repository of the Max Planck Society once the paper is accepted.

*Author contributions.* JSVS: Design experments, perform analyses, write paper; DP: Co-design experiments, perform experiments; CH: write paper

*Competing interests.* No competing interests are present

*Acknowledgements.* We thank Katharina Stolla for reading and commenting the paper. This study is funded by the Deutsche Forschungsgemeinschaft (DFG, German Research Foundation) under Germany's Excellence Strategy - EXC 2037 "CLICCS - Climate, Climatic Change, and Society" - Project Number: 390683824. We thank DKRZ for providing the computing resources.

https://doi.org/10.5194/egusphere-2026-1168
Preprint. Discussion started: 18 March 2026


## References

Allen, M. R. and Ingram, W. J.: Constraints on future changes in climate and the hydrologic cycle, Nature, 419, 224–232, https://doi.org/10.1038/nature01092, 2002.

Baldassare, D., Reichler, T., Plink-Björklund, P., and Slawson, J.: Large uncertainty in observed estimates of tropical width from the meridional stream function, Weather and Climate Dynamics, 4, 531–541, https://doi.org/10.5194/wcd-4-531-2023, 2023.

Chemke, R. and Polvani, L.: Opposite tropical circulation trends in climate models and in reanalyses, Nat. Geosci., 12, 528–532, https://doi.org/https://doi.org/10.1038/s41561-019-0383-x, 2019.

Chemke, R. and Polvani, L. M.: Elucidating the Mechanisms Responsible for Hadley Cell Weakening Under 4 × CO2 Forcing, Geophysical Research Letters, 48, e2020GL090 348, https://doi.org/https://doi.org/10.1029/2020GL090348, e2020GL090348 2020GL090348, 2021.

Chemke, R. and Yuval, J.: Human-induced weakening of the Northern Hemisphere tropical circulation, Nature, 617, 529–532, https://doi.org/https://doi.org/10.1038/s41586-023-05903-1, 2023.

Frierson, D. M. W.: The Dynamics of Idealized Convection Schemes and Their Effect on the Zonally Averaged Tropical Circulation, Journal of the Atmospheric Sciences, 64, 1959 – 1976, https://doi.org/10.1175/JAS3935.1, 2007.

Giorgetta, M. A., Brokopf, R., Crueger, T., Esch, M., Fiedler, S., Helmert, J., and et al.: ICON-A, the atmospherecomponent of the ICON Earth systemmodel: I. Model description, Journal of Advances in Modeling Earth Systems, 10, 1613–1637, https://doi.org/10.1029/2017MS001242, 2018.

Held, I. M. and Soden, B. J.: Robust Responses of the Hydrological Cycle to Global Warming, Journal of Climate, 19, 5686 – 5699, https://doi.org/10.1175/JCLI3990.1, 2006.

Hohenegger, C., Korn, P., Linardakis, L., Redler, R., Schnur, R., Adamidis, P., Bao, J., Bastin, S., Behravesh, M., Bergemann, M., Biercamp, J., Bockelmann, H., Brokopf, R., Brüggemann, N., Casaroli, L., Chegini, F., Datseris, G., Esch, M., George, G., Giorgetta, M., Gutjahr, O., Haak, H., Hanke, M., Ilyina, T., Jahns, T., Jungclaus, J., Kern, M., Klocke, D., Kluft, L., Kölling, T., Kornblueh, L., Kosukhin, S., Kroll, C., Lee, J., Mauritsen, T., Mehlmann, C., Mieslinger, T., Naumann, A. K., Paccini, L., Peinado, A., Praturi, D. S., Putrasahan, D., Rast, S., Riddick, T., Roeber, N., Schmidt, H., Schulzweida, U., Schütte, F., Segura, H., Shevchenko, R., Singh, V., Specht, M., Stephan, C. C., von Storch, J.-S., Vogel, R., Wengel, C., Winkler, M., Ziemen, F., Marotzke, J., and Stevens, B.: ICON-Sapphire: simulating the components of the Earth system and their interactions at kilometer and subkilometer scales, Geoscientific Model Development, 16, 779–811, https://doi.org/10.5194/gmd-16-779-2023, 2023.

Kinne, S., O'Donnel, D., Stier, P., Kloster, S., Zhang, K., Schmidt, H., Rast, S., Giorgetta, M., Eck, T. F., and Stevens, B.: MAC-v1: A new global aerosol climatology for climate studies, Journal of Advances in Modeling Earth Systems, 5, 704–740, https://doi.org/https://doi.org/10.1002/jame.20035, 2013.

Lionello, P., D'Agostino, R., Ferreira, D., Nguyen, H., and Singh, M. S.: The Hadley circulation in a changing climate, Annals of the New York Academy of Sciences, 1534, 69–93, https://doi.org/https://doi.org/10.1111/nyas.15114, 2024.

Mauritsen, T., Bader, J., Becker, T., Behrens, J., Bittner, M., Brokopf, R., Brovkin, V., Claussen, M., Crueger, T., Esch, M., Fast, I., Fiedler, S., Fläschner, D., Gayler, V., Giorgetta, M., Goll, D. S., Haak, H., Hagemann, S., Hedemann, C., Hohenegger, C., Ilyina, T., Jahns, T., Jimenéz-de-la Cuesta, D., Jungclaus, J., Kleinen, T., Kloster, S., Kracher, D., Kinne, S., Kleberg, D., Lasslop, G., Kornblueh, L., Marotzke, J., Matei, D., Meraner, K., Mikolajewicz, U., Modali, K., Möbis, B., Müller, W. A., Nabel, J. E. M. S., Nam, C. C. W., Notz, D., Nyawira, S.-S., Paulsen, H., Peters, K., Pincus, R., Pohlmann, H., Pongratz, J., Popp, M., Raddatz, T. J., Rast, S., Redler, R., Reick, C. H., Rohrschneider, T., Schemann, V., Schmidt, H., Schnur, R., Schulzweida, U., Six, K. D., Stein, L., Stemmler, I., Stevens, B., von

https://doi.org/10.5194/egusphere-2026-1168
Preprint. Discussion started: 18 March 2026


Storch, J.-S., Tian, F., Voigt, A., Vrese, P., Wieners, K.-H., Wilkenskjeld, S., Winkler, A., and Roeckner, E.: Developments in the MPI-M Earth System Model version 1.2 (MPI-ESM1.2) and Its Response to Increasing CO2, Journal of Advances in Modeling Earth Systems, 11, 998–1038, https://doi.org/https://doi.org/10.1029/2018MS001400, 2019.

Miura, H., Satoh, M., Tomita, H., Nasuno, T., Iga, S., and Noda, A. T.: A short-duration global cloud-resolving simulation with a realistic land and sea distribution, Geophys. Res. Lett., 34, L02 804, 2007.

Nguyen, H., Evans, A., Lucas, C., Smith, I., and Timbal, B.: The Hadley Circulation in Reanalyses: Climatology, Variability, and Change, Journal of Climate, 26, 3357 – 3376, https://doi.org/10.1175/JCLI-D-12-00224.1, 2013.

Nordeng, E.: Extended versions of the convective parametrization scheme at ECMWF and their impact on the mean and transient activity of the model in the tropics, Research Department Technical Memorandum, 206, 1–41, 1994.

Pikovnik, M. and Zaplotnik, v.: The Changes of the Northern Hadley Cell Strength in Reanalyses and Radiosonde Observations, arXiv:2503.05331v1 [physics.ao-ph], 2025.

Pikovnik, M., Zaplotnik, v., Boljka, L., and Žagar, N.: Metrics of the Hadley circulation strength and associated circulation trends, Weather and Climate Dynamics, 3, 625–644, https://doi.org/10.5194/wcd-3-625-2022, 2022.

Putrasahan, D. A., Gutjahr, O., Haak, H., Jungclaus, J. H., Lohmann, K., Roberts, M. J., and von Storch, J.-S.: Effect of Resolving Ocean Eddies on the Transient Response of Global Mean Surface Temperature to Abrupt 4xCO2 Forcing, Geophysical Research Letters, 48, e2020GL092 049, https://doi.org/https://doi.org/10.1029/2020GL092049, e2020GL092049 2020GL092049, 2021.

Reick, C. H., Gayler, V., Goll, D., Hagemann, S., Heidkamp, M., Nabel, J. E. M. S., Raddatz, T., Roeckner, E., Schnur, R., and Wilkenskjeld, S.: JSBACH 3 - The land component of the MPI Earth System Model: Documentation of version 3.2, Berichte zur Erdsystemforschung, 240, https://doi.org/10.17617/2.3279802, 2021.

Satoh, M., Tomita, H., Miura, H., Iga, S., and Nasuno, T.: Development of a global cloud resolving model – a multi-scale structure of tropical convections, J. Earth Simulator, 3, 11–19, 2005.

Simpson, I.R.and Shaw, T., Ceppi, P., Clement, A., Fischer, E., Grise, K., Pendergrass, A., Screen, J., Wills, R., Woollings, T., Blackport, R., Kang, J., and Po-Chedley, S.: Confronting Earth System Model trends with observations, Sci Adv., p. PMID: 40073142; PMCID: PMC11900882, https://doi.org/10.1126/sciadv.adt8035, 2025.

Smagorinsky, J., Manabe, S., and Holloway, J. L.: Numerical results from a nine-level general circulation model of the atmosphere, Monthly Weather Review, 93, 727 – 768, https://doi.org/10.1175/1520-0493(1965)093<0727:NRFANL>2.3.CO;2, 1965.

Stachnik, J. P. and Schumacher, C.: A comparison of the Hadley circulation in modern reanalyses, Journal of Geophysical Research: Atmospheres, 116, https://doi.org/https://doi.org/10.1029/2011JD016677, 2011.

Tiedtke, M.: A Comprehensive Mass Flux Scheme for Cumulus Parameterization in Large-Scale Models, Monthly Weather Review, 117, 1779 – 1800, https://doi.org/10.1175/1520-0493(1989)117<1779:ACMFSF>2.0.CO;2, 1989.

Williams, A. I. L. and Jeevanjee, N.: A Robust Constraint on the Response of Convective Mass Fluxes to Warming, Journal of Advances in Modeling Earth Systems, 17, e2024MS004 695, https://doi.org/https://doi.org/10.1029/2024MS004695, e2024MS004695 2024MS004695, 2025.

Zängl, G., Reínert, D., Ripodas, P., and Baldauf, M.: The ICON (ICOsahedral Non-hydrostatic) modelling framework of DWD and MPI-M: Description of the non-hydrostatic dynamical core, Quart. J. Roy. Meteor. Soc., 141, 563 – 579, 2015.

Žiga Zaplotnik, Pikovnik, M., and Boljka, L.: Recent Hadley Circulation Strengthening: A Trend or Multidecadal Variability?, Journal of Climate, 35, 4157 – 4176, https://doi.org/10.1175/JCLI-D-21-0204.1, 2022.